Developmental Biology 411 (2016) 101–114

Contents lists available at ScienceDirect

Developmental Biology

journal homepage: www.elsevier.com/locate/developmentalbiology

Pronephric tubule morphogenesis in zebrafish depends on Mnx mediated repression of *irx1b* within the intermediate mesoderm

Elisabeth Ott [a], Björn Wendik [b,2], Monika Srivastava [b,1], Frederic Pacho [a], Sonja Töchterle [a], Willi Salvenmoser [c], Dirk Meyer [a,*]

[a] Institute for Molecular Biology/CMBI, University of Innsbruck, Technikerstr. 25, 6020 Innsbruck, Austria
[b] Developmental Biology, Institute Biology 1, University of Freiburg, Hauptstrasse 1, 79104 Freiburg, Germany
[c] Institute of Zoology/CMBI, University of Innsbruck, Technikerstr. 25, 6020 Innsbruck, Austria

ARTICLE INFO

Article history:
Received 11 May 2015
Received in revised form
21 September 2015
Accepted 9 October 2015
Available online 22 October 2015

Keywords:
mnx1
mnx2b
irx1b
Sacral agenesis
Currarino syndrome
Intermediate mesoderm
Pronephros
Zebrafish
Development

ABSTRACT

Mutations in the homeobox transcription factor MNX1 are the major cause of dominantly inherited sacral agenesis. Studies in model organisms revealed conserved *mnx* gene requirements in neuronal and pancreatic development while Mnx activities that could explain the caudal mesoderm specific agenesis phenotype remain elusive. Here we use the zebrafish pronephros as a simple yet genetically conserved model for kidney formation to uncover a novel role of Mnx factors in nephron morphogenesis. Pronephros formation can formally be divided in four stages, the specification of nephric mesoderm from the intermediate mesoderm (IM), growth and epithelialisation, segmentation and formation of the glomerular capillary tuft. Two of the three *mnx* genes in zebrafish are dynamically transcribed in caudal IM in a time window that proceeds segmentation. We show that expression of one *mnx* gene, *mnx2b*, is restricted to the pronephric lineage and that *mnx2b* knock-down causes proximal pronephric tubule dilation and impaired pronephric excretion. Using expression profiling of embryos transgenic for conditional activation and repression of Mnx regulated genes, we further identified *irx1b* as a direct target of Mnx factors. Consistent with a repression of *irx1b* by Mnx factors, the transcripts of *irx1b* and *mnx* genes are found in mutual exclusive regions in the IM, and blocking of Mnx functions results in a caudal expansion of the IM-specific *irx1b* expression. Finally, we find that knock-down of *irx1b* is sufficient to rescue proximal pronephric tubule dilation and impaired nephron function in *mnx*-morpholino injected embryos. Our data revealed a first caudal mesoderm specific requirement of Mnx factors in a non-human system and they demonstrate that Mnx-dependent restriction of IM-specific *irx1b* activation is required for the morphogenesis and function of the zebrafish pronephros.

1. Introduction

The vertebrate kidney is an intermediate mesoderm (IM) derived excretory organ with essential functions in blood filtration and ion homeostasis. The common basic structural and functional unit of all vertebrate kidneys is the nephron. It is comprised of a proximal blood filtering glomerulus, followed by an elongated tubular epithelium which leads distally into the terminal collecting duct. Along the proximal-distal axis the tubular epithelium is further divided into segments with specific histology and unique functional properties such as water or ion absorption, pH regulation or solute transport. Although kidney formation has been intensively studied to decipher mechanisms of epithelial branching, segmentation and boundary formation, how the tubular epithelium is formed and segmented is currently not well understood.

The number of nephrons among organisms is variable with more than a million assembled to form some mammalian metanephros, while only one pair of nephrons comprises the pronephros in larvae of amphibians and fish. Amniote pronephros and mesonephros are transient non-functional kidneys that are ultimately replaced by the adult metanephros. In contrast blood filtration and osmoregulation are already functional in the fish pronephros. Despite the much simpler organization of the larval kidney, comparison between mammals and model organisms such as zebrafish suggests that pronephric and metanephric nephrons are composed of the same cell types and their formation is

* Corresponding author. Fax: +43 51250728.
E-mail addresses: elisabeth.ott@uniklinik-freiburg.de (E. Ott), bjoern.Wendik@PERKINELMER.COM (B. Wendik), monika.srivastava@anu.edu.au (M. Srivastava), frederic.pacho@uibk.ac.at (F. Pacho), willi.salvenmoser@uibk.ac.at (W. Salvenmoser), dirk.meyer@uibk.ac.at (D. Meyer).
[1] Current address: Immunogenetics laboratory, John Curtin School of Medical Research, Australian National University, Canberra 2601, Australia.
[2] Current address: PerkinElmer LAS GmbH, Ferdinand Porsche, Juegesheim, Ring 17, D-63110 Rodgau, Germany.

http://dx.doi.org/10.1016/j.ydbio.2015.10.014

regulated by highly conserved signaling pathways and transcription factor networks (Drummond, 2003; Wingert and Davidson, 2008; Wingert et al., 2007). Based on the broad range of genetic, embryological and *in vivo* imaging methods, we used the zebrafish pronephric kidney as a relevant model for kidney development and function.

Formation of the pronephros is divided in four stages, (1) specification of nephric mesoderm from the IM, (2) growth and epithelialisation, (3) nephron segmentation and (4) formation of the glomerular capillary tuft (Drummond, 2003). In zebrafish, the IM is specified during gastrulation (6–10 h post fertilization, hpf). With onset of somitogenesis (11 hpf), different progenitor lineages within the IM can be distinguished based on the expression of pronephric (*pax2.1*) and hematopoietic (*gata1/2*) specific transcription factors. These cell lineages separate during gastrulation and migrate in adjacent, non-overlapping domains between the paraxial and lateral plate mesoderm (Drummond, 2003; Warga et al., 2009). Between the 14 and 22 somite stage the outer pronephric progenitor cells aggregate, undergo a mesenchyme-to-epithelia transition and form the tubular epithelium of the nephric tubule and duct (Gerlach and Wingert, 2014). At 24 hpf, segmentation of the tubule is evident by the restricted expression of various transcription factors and ion-transporters at specific anterior-posterior positions (Serluca and Fishman, 2001; Wingert and Davidson, 2008, 2011; Wingert et al., 2007). Finally, at 48hpf, the glomerulus is connected to the tubules and the kidney is functional (Drummond, 2003).

Previous studies found a requirement for transcription factors of the Iroquois family on morphogenesis and patterning of the vertebrate nephron. Murine *Irx* genes 1–3 were detected in distinct domains of the embryonic as well as adult metanephric kidney (Heliot et al., 2013; Houweling et al., 2001; Massa et al., 2013; Reggiani et al., 2007). While *Irx1* was determined in specific proximal and distal segment domains, *Irx3* was found restricted to posterior proximal segment domains. Consistent with conserved requirements in nephron segmentation, loss of *Irx* functions in mouse, Xenopus and zebrafish interferes with positioning and expansion of intermediate and distal tubule segments (Alarcon et al., 2008; Houweling et al., 2001; Reggiani et al., 2007; Wingert and Davidson, 2011). In zebrafish, *irx3b* expression during mid-somitogenesis regulates differentiation of distal early nephron elements and formation of the proximal segment boundary (Marra and Wingert, 2014; Wingert and Davidson, 2011). While nephric requirements were described predominantly for *Irx3* in the context of segmentation, studies in Xenopus revealed activities of *Irx1* and Irx3 during two different stages of pronephros development. In addition to functions in tubule patterning, an earlier expression of *irx1* and *Irx3* was found to control size and maintenance of the pronephric territory during early nephric specification (Alarcon et al., 2008).

As Irx proteins were initially found in neural tissue, their molecular mechanism of action was predominantly studied during neuron identity determination. It was shown that Irx transcription factors were required for neuron identity specification as well as patterning processes in the developing neuroectoderm (Bellefroid et al., 1998; Bosse et al., 1997; Cavodeassi et al., 2001; Gomez-Skarmeta and Modolell, 2002). The analyses on Irx function in the spinal cord identified Irx3 as a component of a cross-repressive transcriptional network downstream hedgehog signaling that establishes specific neural progenitor domains in the ventral neural tube (Briscoe et al., 2000; Jessell, 2000; Muhr et al., 2001). In particular, Irx3 was found to establish interneuron identity by the repression of motoneuron specifying factors like *Olig2* or *Mnx1 (formerly called hb9 or hlxb9)* (Lee et al., 2008). On the contrary, so far there is only little insight on the non-neuronal transcriptional regulation of *Irx* genes.

We here provide evidence for a direct regulation of early IM-specific *irx* gene expression by Mnx factors. Mutations in the only human *mnx* gene *MNX1* are the major cause of the dominantly inherited Currarino Syndrome, a severe disorder that is characterized by sacral agenesis and various anorectal abnormalities (Belloni et al., 2000; Cretolle et al., 2008; Cretolle et al., 2006; Kochling et al., 2001; Ross et al., 1998). While effected tissues in these patients are mainly of mesoderm origin, so far no evidence for mesodermal Mnx-activities could be identified. In earlier studies the zebrafish *mnx* class genes *mnx1* and *mnx2b* were shown to transiently localize to the lateral mesoderm during early somitogenesis (Lecaudey et al., 2005; Wendik et al., 2004). We show that these *mnx* genes are expressed in distinct domains of the IM and that *mnx2b* expression is restricted to the caudal pronephric mesoderm. Further we show that timing of *mnx* expression coincides with *irx1b* during early stages of pronephric development, while it precedes that of *irx3* expression during tubule segmentation. We demonstrate that Mnx factors repress *irx1b* expression in a cell-autonomous and translation-independent fashion and that this repression is required to restrict *irx1b* activity within the IM. Using knock-down and transgenic gain-of-function approaches we further revealed a specific requirement of *mnx2b* in tubule morphogenesis and we show that knockdown of *irx1b* rescues the pronephric phenotype of the *mnx* morpholino injection.

2. Results

2.1. Expression of mnx genes in the intermediate mesoderm during early somite stages

In previous analyses we determined comparable and divergent spatial and temporal expression patterns in derivatives of all three germ layers for the three zebrafish *mnx* genes, *mnx1, mnx2a and mnx2b (formerly called hb9, mnr2a and mnr2b)* (Wendik et al., 2004). Expression of *mnx1* and *mnx2b* mRNA can be observed from 10 hours post fertilization (hpf) on in the notochord as well as in posterior endodermal cells. With onset of somitogenesis additional expression appears in lateral mesoderm domains (Fig. 1A and D). Co-labeling with the somatic mesoderm marker *paraxial protocadherin* (*papc*) revealed expression of both *mnx* genes lateral to presomitic mesoderm in overlapping but not identical domains. Between the 2 and 10 somite stage *mnx2b* expression appears in bilateral stripes of cells parallel but not directly adjacent to *papc* (Fig. 1A–C). *Mnx1* expression is more dynamic. At early somite stages, staining is found directly adjacent to that of *papc* (Fig. 1D). At the 5 somite stage, the domain of *mnx1* expression broadens laterally, and at 10 somites few *mnx1*-positive cells localize directly adjacent to *papc*, while the majority of *mnx1* positive cells are found in a more lateral position (Fig. 1E and F).

Expression of *mnx1* and *mnx2b* correlates with the position of the IM composed of vascular, blood and kidney progenitor cells. To more precisely identify the *mnx*-positive cells within the IM, expression was compared to the pronephros marker *pax2a* and the blood marker *gata1* by two color *in situ* hybridization. Expression of *mnx2b* was found in *pax2a* positive cells but not in *gata1* positive cells (Fig. 1G, G′, H and H′). By contrast, the majority of *mnx1* expressing cells express neither *pax2a* nor *gata1* (Fig. 1I and J′, data not shown). While the posterior *mnx1* signals in 2 somite stage embryos localize within the *pax2a* positive domain, *mnx1* expression at more anterior positions is found medial to *pax2a*. At the 5 and 10 somite stage a small portion of the *mnx1* positive cells is found directly medial to kidney progenitors (white arrow in Fig. 1E–J) while the majority of *mnx1* expression is found lateral to or intermingled with *gata1* expression (black arrow in Fig. 1 J). In summary, these results reveal kidney progenitor-restricted

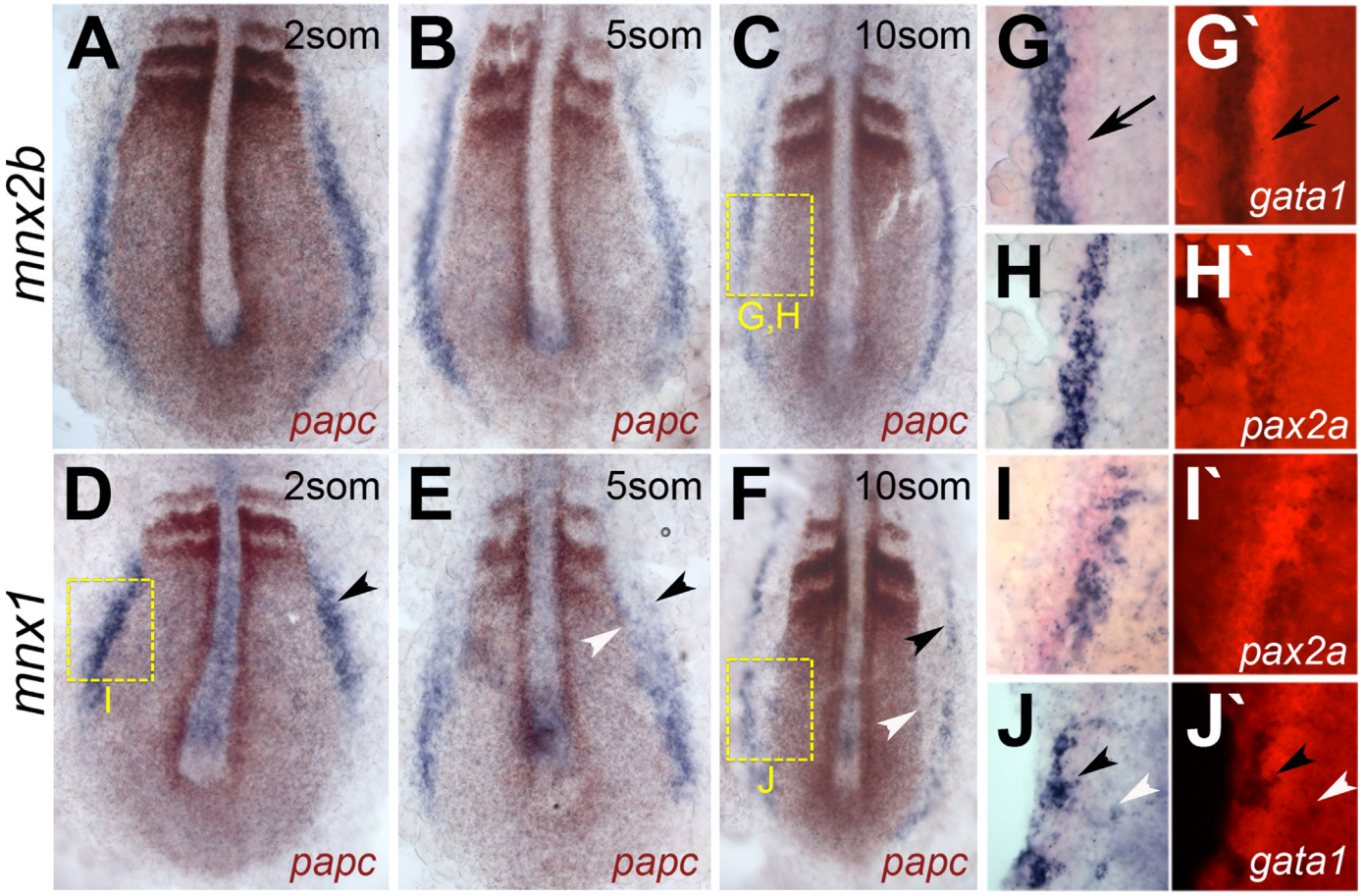

Fig. 1. Distinct expression patterns for *mnx2b* and *mnx1* in intermediate mesoderm. (A–F) Flat-mounts of embryos co-stained for *mnx* genes (blue) and *papc* (brown). Expression of *mnx2b* (A–C) and *mnx1* (d–F) in the IM is present in 2 somite (A, D), 5 somite (B, E) and 10 somite stage (C,F) embryos. Black arrows point to the *gata1* signal, black arrowheads indicate the lateral edge of *mnx* staining, white arrowheads the medial edge of *mnx1* staining. Note that anterior *mnx1* signals at 5 and 10 somite stage forms a lateral (black arrowhead) and a medial stripe (white arrowhead). Yellow boxes indicate positions of higher resolution images shown in G–J. (G–J) Double-ISH stainings for *mnx* genes (blue) with intermediate mesoderm markers (red) for nephrogenic (*pax2.1;* G–I) and hematopoietic cell lineages (*gata1*; J, J′). Shown are brightfield (G, H) and fluorescence images (G′–J′). *Mnx2b* expression is excluded from *gata1* labeled hematopoietic regions (arrow in G, G′), but completely overlaps with the pronephric marker *pax2.1* (H, H′). In contrast, *mnx1* signals are flanking or intermingled with signals for *pax2.1* (2 somite stage; I, I′) and *gata1* (10 somite stage, J, J′).

expression of *mnx2b* and distinct expression of *mnx1* predominantly in *pax2a/gata1* double negative IM cells.

2.2. Normal tubule segmentation in embryos with increased and reduced mnx activities

The temporal restriction of *mnx2b* expression in the pronephric mesoderm correlates with potential functions in pronephric tubule specification, segmentation or epithelialisation. To determine whether *mnx* genes are required for tubule formation, we used *mnx*-morpholino knock-down (for details see Section 4) and transgenic gain- and loss-of-function approaches. Analyses of *pax2a* expression in 24hpf *mnx1*/*mnx2b* single or double knockdown embryos showed no significant defects in pronephros specification (data not shown). To determine defects in tubule segmentation, knock-down embryos were stained at 2 days post fertilization (dpf) with markers for the proximal convoluted tubule (PCT: *slc20a1a*), the proximal straight tubule (PST: *trpm7*), as well as the distal early (DE: *slc12a1*) and late (DL: *slc12a3*) domains (Fig. S1A–D). All pronephric segment markers tested were present in *mnx1*/*mnx2b* single or double knockdown embryos and their positioning in relation to the somite boundaries was similar to control animals (Fig. S1E–H). Measurement of signal lengths also revealed no significant changes in morpholino-injected embryos (Fig. S1Q). In an alternative approach to determine Mnx activities in tubule segmentation, we used transgenic fish lines that produce a conditional induction of Mnx1 (*tg[hsp:mnx1;hsp:YFP]*) alone or a fusion protein of Mnx1 with the viral transactivation domain VP16 (*tg[hsp:mnx1-VP16;hsp:YFP]*), under the control of a heat-shock promoter (hsp70) (Fig. S2). Based on the reported transcription-repressing activities of Mnx proteins (Broihier and Skeath, 2002; Lee et al., 2008; Thaler et al., 1999; William et al., 2003), the induction of *mnx1-VP16* in *Tg(hsp:mnx1-VP16;hsp:YFP)* should counteract endogenous Mnx activities by activating target gene expression, while induction of *mnx1* in *Tg(hsp:mnx1;hsp:YFP)* was expected to further decrease target gene expression. 2dpf transgenic embryos heat-activated at the onset of IM-specific *mnx* expression (1–2 somite stage) revealed slightly shortened expression domains for *slc20a1a*, *trpm7*, *slc12a1* and *slc12a3* as compared to YFP-negative sibling control embryos (Fig. S1I–P). However, the reduced signal correlated with a general reduction of body length of the *mnx1* and *mnx1-VP16*-expressing animals, indicating that segment patterning is normal in these embryos (Fig. S1R). Together, this shows that pronephric tubule induction and segmentation occurred independently of *mnx* gene activities.

2.3. Specific requirement of mnx2b in pronephros morphogenesis and function

As timing of *mnx* gene expression also correlates with nephric duct epithelialization, we further compared duct morphology of

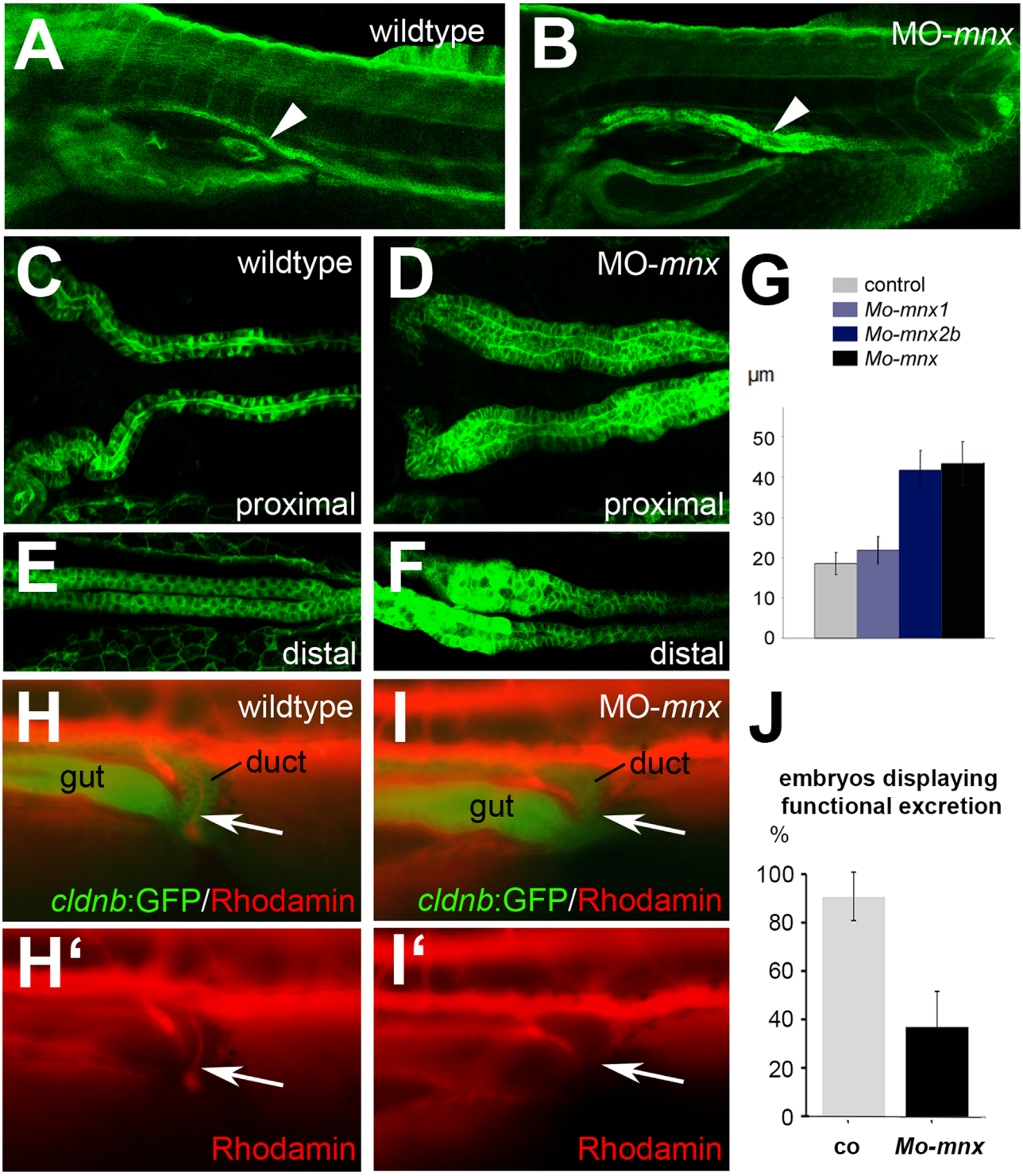

Fig. 2. Mnx2b knock down causes proximal pronephric tubule dilation and excretion defects. (A, B) Lateral views of 4dpf *Tg(cldnb:lynGFP)* control (A) and *mnx1/mnx2b* morpholino injected embryos (single plane confocal image, proximal tubule is indicated by white arrowheads). (C–F) Dorsal views of proximal tubule segments (C, D) as well as proximal to distal transition domains (E, F) in 2dpf *Tg(cldnb:lynGFP)* control (I, J) and morpholino injected embryos. (G) Tubule width in control, single and combined morpholino injected embryos at 4dpf. (H, I) Excretion of rhodamine dextran after injection into the common cardinal vein in controls (H, H′) and *mnx*-morphant (I, I′) *Tg (cldnb:lynEGFP)* embryos at 3dpf (lateral view, white arrows indicate position of duct lumen). 92% of controls showed excretion 5min after injection, compared to only 35% of *Mo-mnx* injected embryos (P).

control and *mnx1/mnx2b* morphant embryos. To better visualize the ducts, we injected corresponding morpholinos into *Tg (-8cldnb.1:lynEGFP)*^{zf106} transgenic embryos in which all epithelia are labeled by membrane tagged EGFP (Haas and Gilmour, 2006). At 4 dpf, morpholino injected embryos displayed severely enlarged tubule width as compared to control embryos (Fig. 2A and B). Remarkably, the tubule dilations in morphant embryos were restricted to proximal domains, while distal segments appeared unaffected (Fig. 2C–F). Specificity of dilation defects to the loss of *mnx2b*-activity was confirmed by a second non-overlapping *mnx2b*-specific morpholino (Fig. S3).

To determine individual roles of *mnx* genes, tubule diameter

were further measured in single morpholino injected *Tg(-8cldnb.1:lynEGFP)zf106* embryos (Fig. 2G, Fig. S3A). Embryos injected with *mnx1* morpholino showed no obvious changes in proximal straight tubule diameter at 4 dpf (21.8 µm, $n=10$) when compared to control embryos (20.5 µm, $n=8$). Differently, tubule width was significantly increased in *mnx2b* morphant (42 µm, $n=25$) and in *mnx1/mnx2b* double morphant embryos (43 µm, $n=12$). Notably, the combined knockdown of both *mnx* genes had no aggravating effect on the tubule width phenotype as compared to *mnx2b* morphants.

To further examine if the tubule dilation observed in *mnx* morphants correlates with impaired kidney function, we used a previously described method for analysis of fluid excretion (Kramer-Zucker et al., 2005). Rhodamin-dextran was injected into the common cardinal vein of control and *mnx*-morphant *Tg(-8cldnb.1:lynEGFP)zf106* embryos at 3.5 dpf and excretion was monitored by fluorescence microscopy. While 92% of uninjected ($n=25$) and control morpholino injected embryos ($n=23$) showed fluid excretion roughly 5 minutes after fluorescent label injection, in 65% of *mnx* morphants we did not observe exrection after 5 min and 59% of the embryos showed no excretion after 20 min ($n=56$) (Fig. 2H–J).

In conclusion the data reveal a specific requirement of *mnx2b* but not *mnx1* pronephric duct morphogenesis and function.

2.4. Mnx-morphants display defects in cilia arrangement and apical microvilli morphology

Tubule dilation has been associated with a wide range of causes within but also outside the nephron (Vasilyev et al., 2009; Gerlach and Wingert, 2014). Reduced excretion can depend on changes in heart or glomerular functionality. However, *mnx2b* morphant embryos had a normal heart beat rate, no heart edema were observed (Fig. S3B–D) and glomerular histology appeared normal

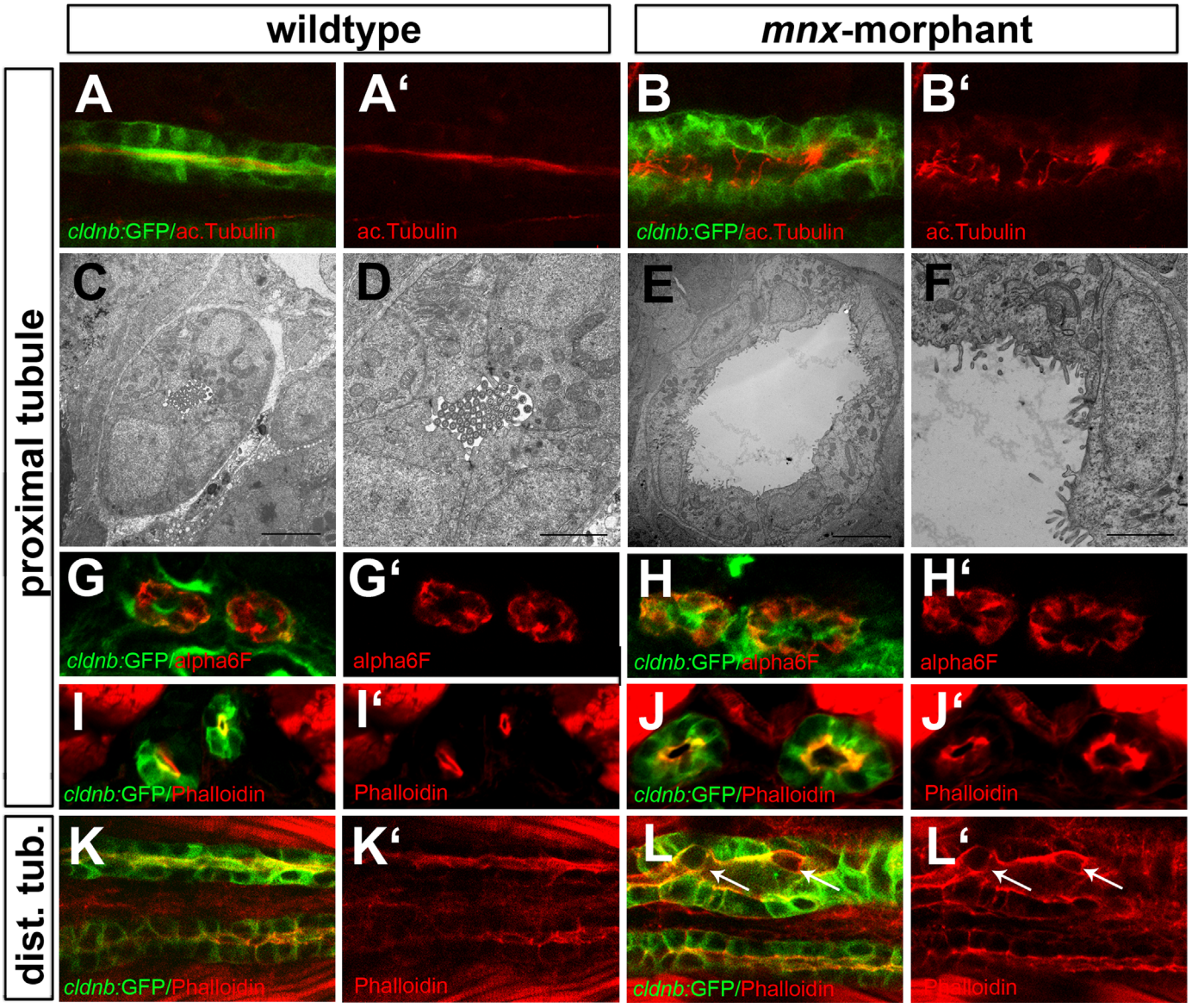

Fig. 3. Mnx knockdown causes defects in tubular cilia arrangement and epithelial morphology. (A, B) Single plane confocal images showing tubule cilia stained by anti-actelytaled tubulin (red). Shown are lateral views of proximal tubules of control (A, A′) and *mnx*-morpholino injected *Tg(cldnb:lynGFP)* embryos (B, B) (C–F) Transverse TEM sections of proximal tubules in control (C, D) and *mnx*-morpholino embryos (E, F). Note disorganized microvilli structures after *mnx* gene knockdown (scale bars correspond to 5 µm (C, E) and 2 µm (D, F)). (G–J) Transverse sections of proximal tubules in control and *mnx* morphant embryos at 2dpf. Staining of baso-lateral surface directed alpha6F (G, H) and apically located Phalloidin (I, J) displayed similar expression patterns in control and MO-*mnx*. (K, L) Single plane confocal images of distal tubules stained for Phalloidin (red, ventral view). White arrows indicate displaced epithelial cells with unpolarized Phalloidin signals.

(Fig. S4). Previous studies demonstrated that excretion defects are primarily caused by defects in ciliogenesis or ciliary function (Kramer-Zucker et al., 2005; Zhao and Malicki, 2007). To test if ciliated cells are specified in *mnx*-morphants, 2 dpf embryos were analyzed for *trpm7* and *shippo1/odf3b* mRNA which label mono-ciliated and multi-ciliated cells, respectively. Whole mount stains revealed indistinguishable patterns of *trpm7* expression and a slightly different pattern but unaffected number of *shippo1/odf3b* positive cells in *mnx*-morphant embryos (on average 46 cells; Fig. S5). To determine if cilia formation itself is affected by the knockdown of *mnx* genes, 4 dpf embryos were further examined with an antibody directed against acetylated tubulin. In control embryos acetylated tubulin labeled cilia arranged in a dense band within the pronephric lumen (Fig. 3A). While cilia bundles were also present in *mnx* morphants, their extensions into the dilated pronephric lumen appeared somewhat disorganized (Fig. 3B). To determine whether misorientation of cilia is caused by defective cilia motility, we performed short time-lapse movies on proximal tubule regions of control and *mnx* knockdown embryos. This experiment showed beating cilia in *mnx* morphants, although the available resolution did not allow interpretation of effects on cilia beat rate (data not shown). To further exclude cilia defects in *mnx* morphant embryos, sections of 2 dpf control and *mnx* morphant proximal tubules were investigated by transmission electron microscopy (TEM, Fig. 3C–F). These analyses revealed normal 9+2 ciliary architecture in *mnx* morpholino injected embryos (Fig. S6). In conclusion this suggests that neither the formation of specific ciliated cell types nor functionality of cilia itself is affected by a loss of *mnx* functions.

In the TEM analyses we recognized deformed and disorganized microvilli structures at the apical side of dilated tubules (Fig. 3C′ and F′). To test if the abnormal microvilli organization might be caused by defects in cell polarity we labeled embryos with Phalloidin and alpha6F antibodies to mark apical actin and basolateral localized Na^+/K^+ ATPase.

Transverse sections of dilated tubules in *mnx* morpholino-injected embryos showed disturbed epithelial cell compaction but in general proper apical and basal localization of Phalloidin-bound actin and alpha6F labeled Na^+/K^+ ATPase, respectively (Fig. 3G–J′). However, when we closely examined Phalloidin staining in the more distal located tubules of morpholino-injected embryos, we noticed cells with an atypical actin-pattern that localized within the tubule lumen (Fig. 3K and L). The data suggest that the tubule dilation in *mnx* morphants is not caused by polarity defects in the dilated proximal segment itself, but could instead be an indirect consequence of lumen occlusion in the distal tubule.

2.5. *Mnx transcriptional repressors regulate expression of iroquois gene irx1b*

Given our findings of a functional role for Mnx2b in the zebrafish kidney, we approached to determine downstream signaling factors in pronephric mesoderm development. To identify Mnx target genes we took advantage of the predicted complementary regulation of Mnx-targets in *Tg(hsp:mnx1;hsp:YFP)* and *Tg(hsp:mnx1-VP16;hsp:YFP)*. By microarray based transcriptome comparison of *mnx1-vp16* induced to wildtype animals we identified 44 transcription factors with at least 1.5-fold change in expression level (p val. < 0.05; Supp. Table S1). Only 16 of these genes showed the expected upregulation by *mnx1-VP16*, indicating a large

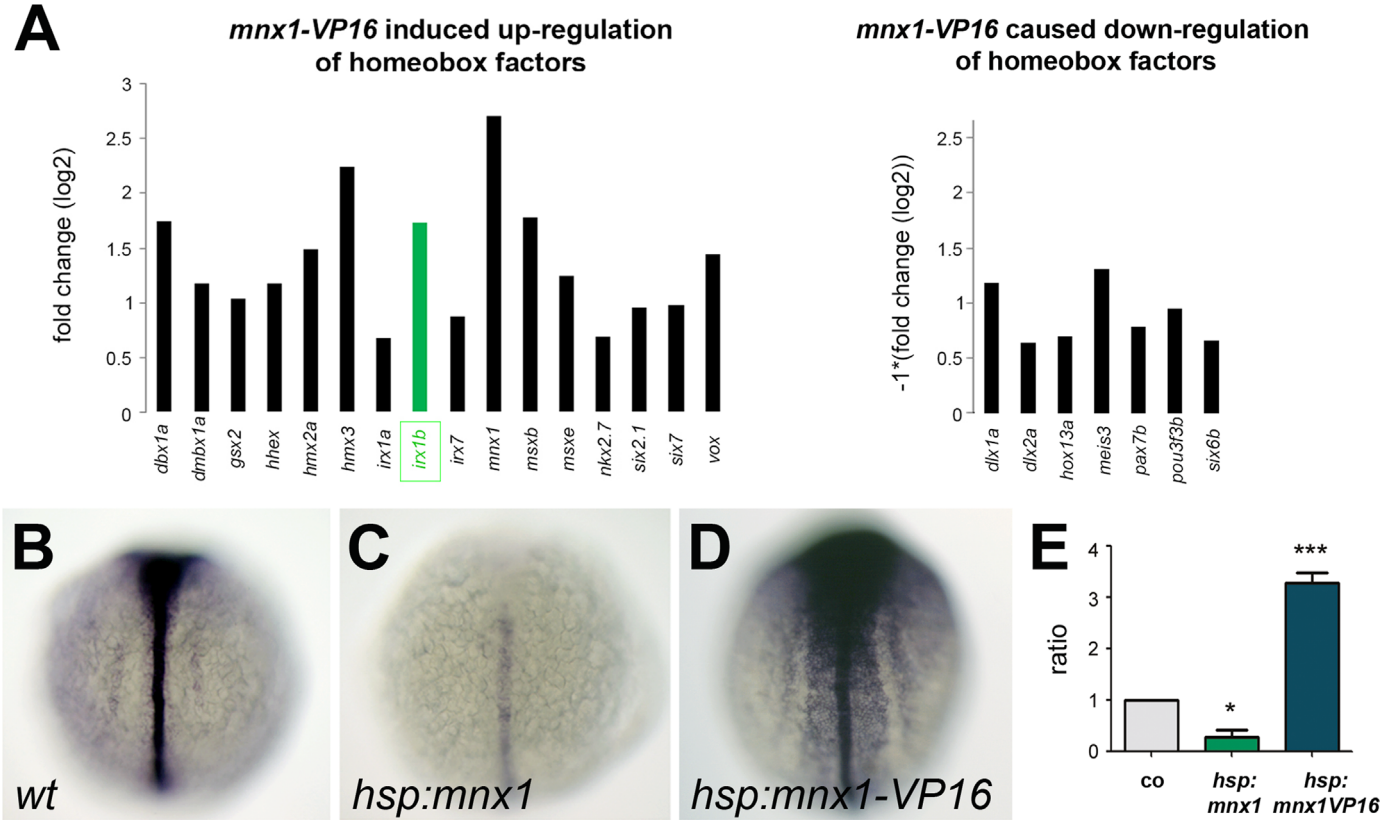

Fig. 4. Mnx1 negatively regulates *irx1b* expression. Microarray analysis identified differential expression of homeobox-containing genes in *mnx1-VP16* induced animals compared to wild type controls. Genes attributed with the GO terms transcription regulation and homeobox that have increased expression in *mnx1-VP16* animals are indicated (note that the robust *mnx1* induction corresponds to the induced *mnx1-VP16* transcripts). Shown are genes with > 1.5 fold increase or reduction in expression after *mnx1-VP16* activation (A). Of three identified *irx* family genes, *irx1b* showed the highest change in expression (labeled in green). Whole mount *in situ* hybridization for *irx1b* in wild type controls (B), *mnx1* induced (C) and *mnx1-VP16* induced (D) embryos, dorsal view. Negative regulation of *irx1b* through Mnx1 was further confirmed in qPCR analysis (E; p val < 0.05 (*), < 0.001 (***)).

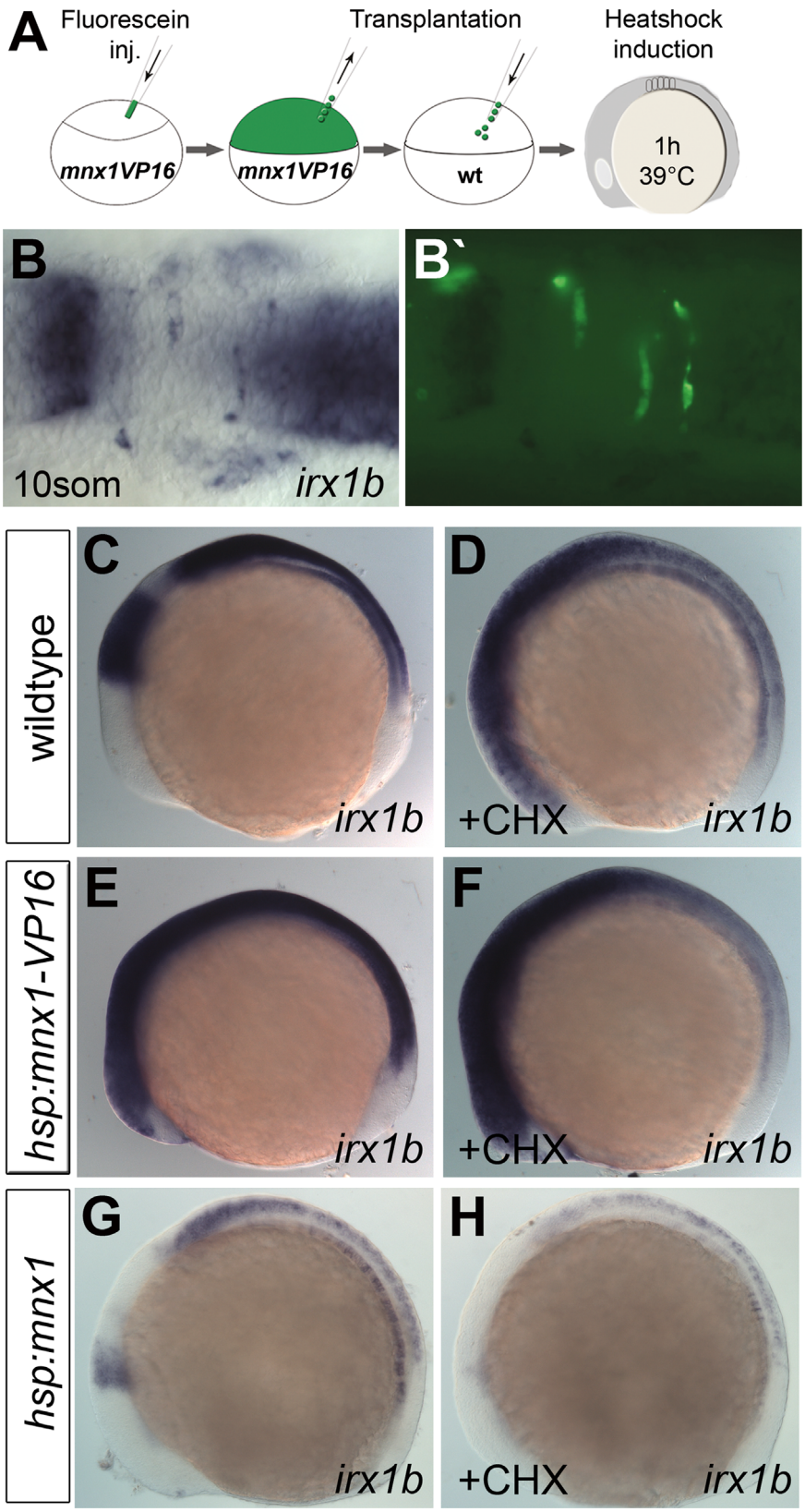

Fig. 5. Direct transcriptional repression of *irx1b* through Mnx factors. Outline of the transplantation experiment. Mnx1VP16 embryos are injected with fluorescein dextran at the 1-cell stage. Fluorescein positive cells are transplanted into wt embryos during shield stage. Embryos are fixed 2h after 1h inductive heat-activation and analysed for fluorescein and *irx1b* expression (A). Transplanted transgenic cells ectopically express *irx1b* (B, B′). Lateral view of *irx1b* stained wt embryos is shown (C) and after CHX treatment (D). *Irx1b* expression is similarly induced in *mnx1-VP16* expressing embryos (E, F), and similarly reduced in *mnx1 overexpressing* embryos (G, H) without or with CHX, respectively.

fraction of indirectly regulated target genes. However, among the *mnx1-VP16* induced genes were members of the Iroquois transcription factor family with previously described crucial roles in kidney development (Fig. 4A and Supp. Table S1) (Alarcon et al., 2008; Cheng et al., 2007; Lecaudey et al., 2005; Rodriguez-Seguel et al., 2009; Stedman et al., 2009; Wingert and Davidson, 2011). In particular, the array analyses revealed minor *mnx1-VP16* induction for *irx1a* and *irx7*, and a very prominent induction for *irx1b* (3.3 fold induced expression in activated animals compared to wild type controls, Fig. 4A and Supp. Table S1). Regulation of *irx* genes was further analysed by quantitative reverse transcriptase PCR (qPCR) analysis and whole mount *in situ* analyses of 12 hpf embryos heat-treated at 10 hpf. The qPCR studies confirmed a 3.7 fold reduction of *irx1b* mRNA in *mnx1* induced animals and a 3.3 fold increase in *mnx1-VP16* activated animals (Fig. 4E). Whole mount stains revealed a complete loss of intermediate mesoderm-specific *irx1b* expression in *mnx1* induced embryos, while induction of *mnx1-VP16* under the same conditions resulted in robust *irx1b* signals, specifically in intermediate mesoderm and in the nervous system (Fig. 4B–D).

To test for a potential cell-autonomous regulation of *irx1b* by Mnx-factors, we generated embryos with a mosaic activation pattern of either *mnx1-VP16* or *mnx2b-VP16* by using cell transplantation and DNA-injection, respectively. Transplantations were using fluorescein-Dextran injected *Tg(hsp:mnx1-VP16;hsp:YFP)* embryos as traceable donors and wildtype embryos as hosts (schematic Fig. 5A). Chimeric embryos that were heat-treated at 12 hpf and fixed at 14 hpf showed strongest *irx1b* mRNA signals specifically in transplanted fluorescein labeled cells (Fig. 5B). Similarly, ectopic *irx1b* induction was also observed in embryos injected with the Mnx2b-VP16 expression plasmid pCS2-Mnx2b-VP16 (Fig. S7). While most of the Mnx1-VP16 and Mnx2b-Vp16 induced *irx1b* signals were detected in the nervous system, the results revealed similar cell-autonomous effects of both Mnx factors. The data are consistent with either a direct regulation of *irx1b* through Mnx factors or with an indirect regulation through transcriptional activators acting downstream of Mnx-VP16. If the regulation is direct, then *irx1b* induction by Mnx1-VP16 would not be inhibited by the translation blocking agent cycloheximide (CHX). Consistent with this, addition of CHX to Mnx1-VP16 induced embryos shortly after heat-shock treatment at 10 hpf did not prevent *irx1b* induction (Fig. 5C–F) or *irx1b* repression in Mnx1-induced embryos (Fig. 5G and H). These results strongly suggest that *irx1b* transcription is directly repressed by Mnx proteins and that Mnx/*irx1b* interactions are not restricted to intermediate mesoderm but are also relevant in other tissues including the nervous system.

2.6. Complementary IM-specific expression on irx1b and mnx genes

To determine potential interactions of *mnx* and *irx* genes in pronephros formation in more detail we performed expression analyses of zebrafish *irx* genes. Notably, only *irx1* and *irx3* genes were expressed in the developing pronephros. Our analyses confirmed the previously shown pronephric expression of *irx1a* and *irx3b* at 15–20 hpf (Fig. S8) (Lecaudey et al., 2005; Wingert and Davidson, 2011). In addition, they revealed IM specific *irx1b* transcription between 11 and 16 hpf (Fig. S9). Comparison of *irx1b* and *mnx* signals in embyros that were co-stained with the muscle marker *myoD* further revealed mainly non-overlapping expression of *irx1b* and *mnx* genes in IM flanking anterior and posterior somites, respectively (Fig. S9). Specificity of these signals to pronephric mesoderm was confirmed by the overlap of *irx1b* signals with *pax2a* expression (Fig. 6 A). This temporarily overlapping but spatially complementary localization of *irx1b* and *mnx* is consistent with a cross-repressive interaction between Mnx and Irx factors within the pronephric IM. To further examine if Mnx factors are required to restrict *irx1b* expression, we determined *irx1b* mRNA expression in embryos injected with *mnx1* and *mnx2b* morpholinos either alone or in combination at the 8 somite stage. In all *mnx* knockdown experiments we observed a posterior expansion of *irx1b* signals within the IM (Fig. 6B and C). The measurement of the distance from the tailbud to the level of the posterior end of *irx1b* expression revealed expansion of 60 μm in *mnx1* morphants, 90 μm in *mnx2b* morphants and 180 μm in *mnx* morphant embryos (Fig. 6D).

The complementary experiment, analysis of *mnx* expression in *irx1b* morphant embryos, revealed no obvious changes in IM

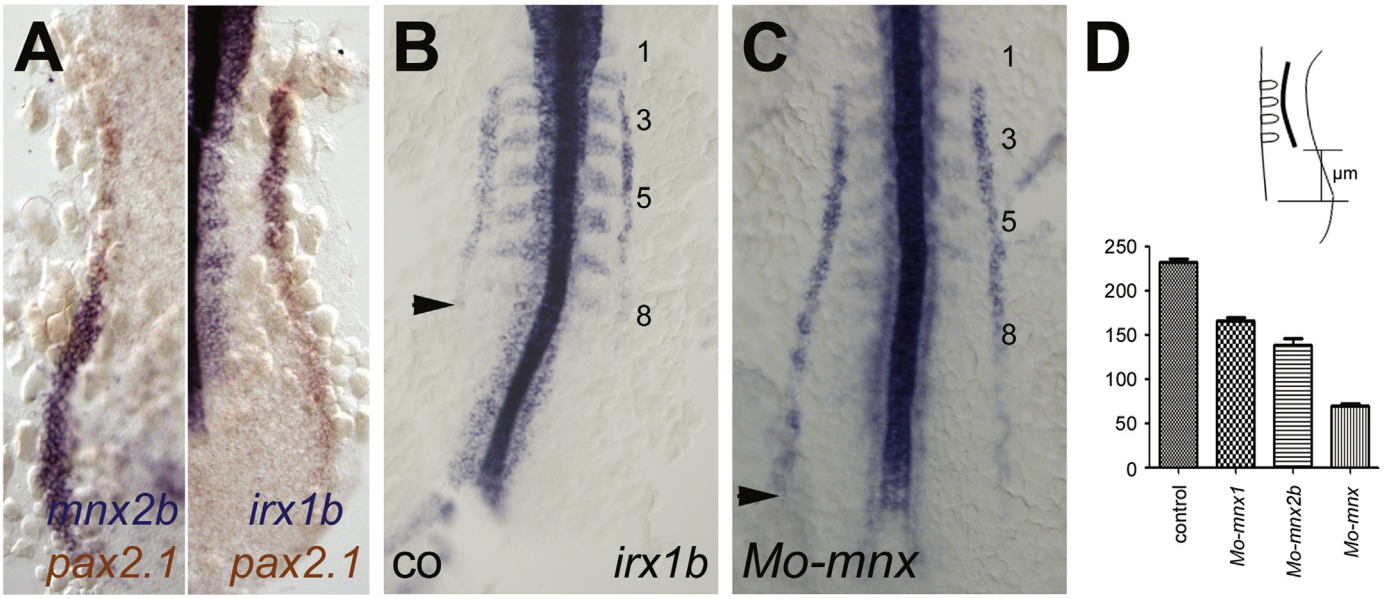

Fig. 6. *Mnx* gene knockdown results in posteriorly expanded expression of *irx1b*. Flat-mount views of wild type and morpholino-injected embryos. Double-ISH analysis for either *mnx2b* or *irx1b* (blue) and *pax2.1* (brown) shows localization within the nephric mesoderm at the 5som stage (A). Mesoderm expression of *irx1b* at the 8som stage is posteriorly expanded in *mnx* morphant embryos (C) compared to controls (B). Arrowheads point to posterior end of *irx1b* signals. Measurements of the distance from the posterior end of *irx1b* signals to the tail-bud are presented for single and double morpholino injected embryos (D).

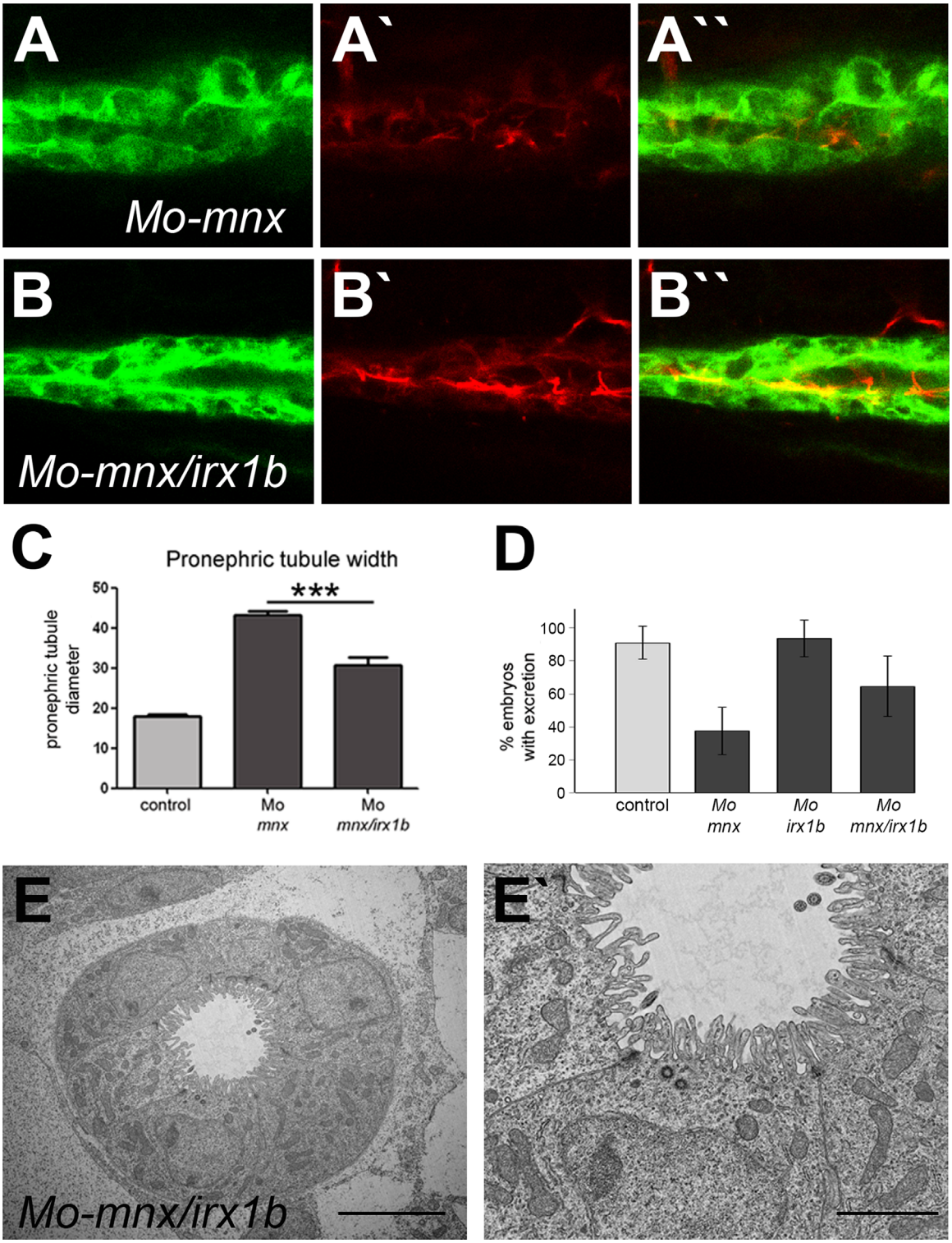

Fig. 7. Knockdown of *irx1b* in *mnx* morphants partially rescues pronephric phenotypes. Shown is a lateral view of Acetylated tubulin stained Tg(cldnb:lynEGFP) embryos that were injected with *Mo-mnx* alone (A, A′) or in combination with *Mo-irx1b* (B, B′). Measurement of tubule widths shows partial rescue of the MO-*mnx* phenotype in the combination *mnx/irx1b* double knockdown (C). Excretory defects in *Mo-mnx* injected embryos are rescued by additional *irx1b* knockdown (D). TEM sections of embryos co-injected for *mnx* and *irx1b* morpholinos demonstrate reduced pronephric tubule width and restored morphology of microvilli (E, E′; Scale bars correspond to 5 and 2 μm, respectively).

specific expression of *mnx1* and *mnx2b*. However, due to strong pleiotrophic effects of *irx1b* morpholino injections, only embryos injected with lower *irx1b* morpholino amounts enabled efficient staging through myoD labeled somites (data not shown). In summary, our results show that Mnx factors repress IM specific *irx1b* transcription and that this activity restricts the extent of *irx1b* expression in the posterior mesoderm.

2.7. *irx1b knock down partially rescues kidney defects in mnx morphants*

The data reveal a correlation between pronephric tubule

defects and posterior expansion of mesodermal *irx1b* signals in *mnx* morpholino injected embryos. If the kidney defects are caused by expanded *irx1b* expression, the knockdown of *irx1b* in *mnx* morpholino injected embryos should rescue the phenotypical defects. Indeed, tubules of embryos co-injected with *irx1b* and *mnx* morpholinos displayed reduced lumen diameter (Fig. 7A and B) and a more compact cilia organization (Fig. 7A′ and B′) as compared to the *mnx* morphants. Measurement of proximal tubule widths at 4 dpf confirmed a significantly reduced tubule diameter (34.5 μm, $n=10$) in *mnx/irx* double morphants as compared to *mnx* morpholino injected embryos (43 μm, $n=10$) (Fig. 7C). In addition, 63% ($n=46$) of the *mnx/irx1b* double morphants showed urinary excretion while this was seen in only 35% of the *mnx* morpholino injected embryos (Fig. 7D, Fig. S10). Further TEM sections of *Mo-mnx/irx1b* injected embryos demonstrated restored morphology of luminal microvilli (Fig. 7E and E′). These data suggest that expanded *irx1b* expression in ventral IM domains is the major cause for the *Mo-mnx* induced kidney phenotypes.

3. Summary and discussion

Our analyses in the model organism zebrafish reveal a novel interaction and requirement for Mnx and Irx transcription factors during early nephrogenesis. We found that *irx1b* and the *mnx* genes *mnx1* and *mnx2b* are expressed in mutually exclusive domains of the IM which later form the pronephric tubule. Using gain and loss of function approaches we showed that this distribution results from repression of *irx1b* by Mnx1 and Mnx2b and we provide evidence for a direct repression. We further show that restriction of *irx1b* expression by Mnx2b is required for normal tubule morphogenesis and proper nephron function.

3.1. Potential functions of Mnx1 in the mammalian kidney

Mutations of *MNX1* in humans were identified as the main cause of the Currarino syndrome, a congenital disease associated with sacral dysgenesis, anorectal malformations and presacral tumors (Cretolle et al., 2006; Kochling et al., 2001; Lynch et al., 2000). These main symptoms are often accompanied by renal and gynecological malformations. The most common urogenital defects in Currarino syndrome patients are vesico-ureteral reflux, hydronephrosis and horseshoe kidneys (Colapinto et al., 2003; Currarino et al., 1981; Iyer and Khanna, 2010).

Initial studies on *MNX1* identified functions in the regulation of progenitor cells into mature hematopoietic cells (Deguchi and Kehrl, 1991; Harrison et al., 1994). Increased *MNX1* levels in acute leukemia patients indicated a contribution to leukemogenesis (Deguchi et al., 1993). The identification of MNX1 regulated genes that are associated with leukemic processes further strengthened this hypothesis (Wildenhain et al., 2012). Recent studies determined elevated *MNX1* levels also in other tumors including colorectal or hepatocellular cancers, suggesting a tumor suppressor function for MNX1 (Cretolle et al., 2008; Hollington et al., 2004; Wilkens et al., 2011). Noteworthy, we found that *mnx1* expression during zebrafish somitogenesis is not overlapping but adjacent to the nephric mesoderm. After random integration of a Mnx1 promoter regulated GFP in mice, Mnx1 was localized within a subset of microvascular blood vessels (Pickles et al., 2013). These studies explicitly demonstrated how important it will be to address the potential roles of MNX1 in endothelial cells and vasculogenesis in greater detail.

In animal models, functional studies on Mnx1 so far mainly focused on its requirement for the differentiation of endocrine pancreatic progenitors and motor neurons (Broihier and Skeath, 2002; Dalgin et al., 2011; Eisen, 1999; Harrison et al., 1999; Li et al., 1999; Seredick et al., 2012; Thaler et al., 1999; Wendik et al., 2004). Little is however known on the molecular functions of Mnx1 in mesoderm derived tissues. The detection of Mnx1 in the tailbud of Xenopus embryos at tadpole stages supported the consideration for a role of Mnx1 in sacrum formation (Ross et al., 1998; Saha et al., 1997). Neural tube defects in caudal agenesis were shown to be restricted to posterior regions (Catala, 2002). However, contrary to presumptions mice mutant for Mnx1 did not show apparent skeletal truncations. It is still unclear, if the lack of caudal defects in the Mnx1 mutant mice results from differences in gene function between human and mice or if the mutations in humans are caused by gain instead of loss of function defects (Catala, 2002).

Despite the frequent observation of renal malformations in Currarino syndrome patients, potential Mnx1 functions in the mammalian kidney were not addressed so far. While the analyses of *Mnx1* mutant mice revealed no evidence for kidney specific requirements, detailed expression analyses localized low level of *Mnx1* transcripts in the lower urinary tract (Brunskill et al., 2008). Characterization of a cre-reporter mouse localized Mnx1 in embryonic and adult kidney tissue (jaxmice.jax.org). We here show that zebrafish *mnx2b* localizes to the nephric mesoderm during somite stages. The striking similarities in the genetic control of the pronephric and metanephric kidney suggest that Mnx activities might be conserved from lower to higher organisms.

3.2. Mnx knockdown results in anterior tubule dilation, cilia disarrangement and impaired excretion

Functional blood filtrating nephrons in zebrafish consisting of glomerulus, tubular elements and collecting duct are formed by 48 hpf (Drummond, 2000; Gerlach and Wingert, 2013). Dysfunctions leading to pronephric tubule dilations are mainly caused by ciliary or glomerular filtration defects (Kramer-Zucker et al., 2005; Sullivan-Brown et al., 2008; Zhang et al., 2012). Intriguingly, in *mnx* morphants cilia arrangement was disorganized in dilated proximal tubule segments and we observed reduced solute excretion. Comparison of beating cilia to control animals showed that function of remaining cilia was not disrupted in *mnx* morphants (data not shown). Further, the normal patterns of mono- and multi-ciliated cell markers in the morphants suggest that neither differentiation nor positioning of ciliated cell types is affected. These results indicated that the defects in cilia arrangement were rather a consequence than the cause of the pronephric phenotype.

3.3. Pronephric tubule occlusion as a prospective cause of the mnx morphant phenotype?

Pronephric growth and tubule convolution require anterior cell migration and posterior proliferation events. Around 30hpf fluid flow initiates pronephric cell migration and subsequently proximal tubules are shortened and convoluted. Occlusion of anterior tubules results in a loss of distally located cell migration and reduced proliferation, while distal tubule obstructions lead to increased cell proliferation and luminal distension (Vasilyev et al., 2012). It was further shown that cell migration induced proliferation in distal tubule segments depends on PI3K and also CDK4/Cyclin D1 signaling (Vasilyev et al., 2012). The observation of less distinct convolution in *mnx* morphant pronephros suggested that cell migration was reduced in embryos exhibiting impaired fluid flow. A role for PI3K signaling in Mnx functions is not known so far.

Knockdown of the zebrafish *polycystin2* (*pkd2*) gene was associated with occlusion dependent pronephric cyst formation (Obara et al., 2006). *Pkd2* morphants exhibit defects similar to *mnx* morphant embryos with proximal tubule dilations and disturbed urine excretion. Cilia morphogenesis and beat rate are not affected by

the knockdown of *pkd2*. Instead, the proximal tubule dilations are caused by occlusions in posterior tubule segments. Mechanical obstruction of the pronephros was further shown to cause cystic dilations only in anterior tubules and not in distal located tubules or the collecting duct (Kramer-Zucker et al., 2005). Based on these studies, we presume that the tubule dilations in *mnx* morphants are caused by obstructions in distal epithelia. In our microarray based identification of Mnx targets no differential expression of *pkd* genes was observed (data not shown), indicating that Mnx actions occur independent or downstream of Pkd signaling. Analysis of mutant fish lines that presented pronephric tubule dilations with different effects on cilia motility indicated the presence of various mechanisms that lead to cyst formation (Sullivan-Brown et al., 2008). Although changes in ciliary function and epithelial polarization were discovered in these mutant lines, so far there is only limited knowledge on the mechanisms causing the tubule dilations. The observation of morphologic alterations at the transition of dilated proximal to unaffected distal tubule segments promotes the idea of a tubule occlusion after *mnx* knockdown. Within these nephron areas we observed malformations in epithelial cell compaction. TEM analysis further supported a defect in actin filament derived microvilli formation. These apical domains are formed during polarization processes in epithelial cells and function in multiple cellular processes like glucose transport regulation, ion channel regulation and membrane potential modulation (Lange, 2011; Mitra et al., 2012; Raschperger et al., 2008).

Through transcriptome comparison of conditional active and negative Mnx1 transgenic zebrafish we identified the Iroquois homologue *irx1b* as Mnx1 target. As knock-down of the *iroquois* homologue *irx1b* in *mnx* morphants could significantly reduce the morphological defects and restore microvilli structures, it is likely that the ventral mesoderm repression of *irx1b* is required for actin related cell compaction processes.

3.4. Kidney formation requires restriction of irx1b in posterior mesoderm domains by Mnx factors

Inhibitory interactions between MNX and IRX homeobox factors have been reported for neural progenitor cells, where IRX factors block *Mnx* genes to promote interneuron cell fates (Lee et al., 2004). Recent reports further associated *Irx/irx* class genes with pronephric cell specification and tubule segmentation. These activities were predominantly associated with *Irx3*, but lately there was also indication for a role of *Irx1* in these processes (Alarcon et al., 2008; Houweling et al., 2001; Reggiani et al., 2007; Wingert and Davidson, 2011). In xenopus independent *Irx* functions at early and late stages of kidney formation were described. While early *Irx1* and *3* signals affected the entire pronephric field, later signals are restricted to intermediate tubule development (Alarcon et al., 2008). Loss of function studies demonstrated a more prominent role to *Xiro3/irx3* (Alarcon et al., 2008; Reggiani et al., 2007). Studies in fish could determine related functions to the *irx* homologue *irx3b*, which was shown to be essential during segmentation processes (Wingert and Davidson, 2011). The knockdown of *irx3b* in zebrafish causes expansion of proximal segments at expense of the distal early segment (Wingert and Davidson, 2011).

Our analyses located the previously found expression of *mnx* genes in ventral mesoderm domains within the pronephric cell lineage anlage. Further we found that mesoderm expression of *mnx* genes coincides with that of *irx1b*, while *irx1a* expression was observed within the pronephric mesoderm at comparable stages as *irx3b*. This suggests that *irx1a* functions are related to the previously described *Xiro1* functions in pronephros segmentation. Therefore, our data demonstrate a requirement for the *irx1* homologue *irx1b* in nephrogenesis that precedes *irx3b* functions.

In our experiments, the repressive activity of Mnx factors predominantly affected *irx1b*. Remarkably, during somitogenesis *mnx* and *irx1b* gene expression was detected in mutual exclusive domains of the IM, with *irx1b* located anterior to *mnx* genes. We show that within the nephric mesoderm Mnx factors prevent zebrafish *irx1b* expansion from anterior into posterior domains. Furthermore, the induced *irx1b* activity after a loss of Mnx function was found to cause proximal tubule dilation and impaired urinary excretion.

Although initial studies on Mnx and Irx interactions suggested a cross-repressive action, *irx1b* knockdown did not cause anterior expansion of *mnx* signals within the IM. Therefore *Irx1b* seems to be either dispensable or not sufficient to regulate IM specific *mnx* expression.

In agreement with previous studies, *Irx1* expression was found in the murine metanephros and lower urinary tract (Reggiani et al., 2007). The localization of both, *Mnx* and *Irx* genes, within the genito-urinary tract of mice further strengthens the idea that the identified *mnx-irx* interaction is not restricted to the simple zebrafish pronephros, but is a conserved feature also in the more complex meso- and metanephros in higher mammals. In conclusion, our analyses provide new clues on the molecular interaction between Mnx and Irx factors and provide a first hint for a mesoderm specific molecular role of the Currarino syndrome factor MNX1.

4. Material and methods

4.1. Transgenic fish lines

Zebrafish (Danio rerio) were raised under standard conditions at 28 °C. AB and TU wild-type strains were used and staged according to Kimmel et al. (1995).

The following lines were used for heat-shock experiments: *Tg (hsp70:mnx1_hsp70:YFP)*, *Tg(hsp70:mnx1-VP16_hsp70:YFP)*. These lines were obtained by injection of hsp70:*mnx1*_hsp70:YFP or hsp70:*mnx1*VP16_hsp70:YFP constructs into wildtype embryos at the 1-cell stage. Positive integration of the constructs was tested *via* heatshock-induced YFP expression and confirmed by ubiquitous induction of *mnx1* expression in whole mount *in situ* hybridization experiments. The *Tg(-8cldnb.1:lynEGFP)zf106* line was used for *in vivo* marking of epithelial structures (Haas and Gilmour, 2006).

4.2. Morpholino injections

Morpholino oligonucleotides (MO) were synthesized by Gene Tools, diluted at a stock concentration of 2 mM (~16 ng/μl) in H2O and stored at −20 °C. Dilutions of 1.5–4 ng/μl of morpholino was injected into one-cell stage embryos. For generating double *mnx* morphants, the concentration of individual morpholinos was halved to keep the total amount of morpholino injected the same as for single morphants. The following antisense morpholinos were used (numbers indicate position relative to underlined start codons).

mnx1: *Mo-mnx1* (−8 to +17: TTTTTAGATTTCTCCATCTGGCCCA); *mnx2b: mnx2b-MO* (*M2b_atgMo2)* (−1 to +24: CCTGAAGTTCTTTGACTTTTCCATT, *Mo-mnr2b2 (MO^{mnr2b})* (-27 to -2: GACTTTTCCATTGCAACACTTTTGT) (Wendik et al., 2004); *irx1b: Mo-irx1b* (−21 to +4: ACATGTCCAACTCCCGAGGAACTCT) (Stedman et al., 2009) and *Mo-irx1b2* (−68 to −43: AGGGCAATCCACTTTCAATCACAGC).

All MO-experiments were initially done with the previously published *Mo-mnx1, mnx2b-MO* and *Mo-irx1b.* In addition, the following experiments were repeated with non-overlapping translation-blocking morpholinos against *mnx2b* (*Mo-mnr2b2)* and

irx1b (Mo-irx1b2): quantification of tubule dilation in mnx2b-single and mnx2b/irx1b-double morphants and analyses of heart beat rates. Importantly, indistinguishable phenotypes were observed for both sets of *mnx2b* and *irx1b* morpholinos,

4.3. Whole mount in situ hybridization

Whole mount *in situ* hybridization (WISH) experiments were performed as described previously (Hauptmann and Gerster, 2000; Thisse et al., 1993; Wendik et al., 2004). Anti-sense RNA probes were prepared by transcribing linearized cDNA clones with SP6 and T7 polymerases using the digoxigenin labeling mix (Roche). Plasmids for ISH probes of *irx* genes and pronephros segmentation markers were obtained from Sylvie Schneider-Maunoury and Alan Davidson, respectively (Lecaudey et al., 2005; Wingert et al., 2007).

4.4. Immunostainings

Antibody staining was performed as previously described (Kimmel et al., 2011). Anti-mouse GFP (Roche) was used in a 1:200 dilution, Alexa 488 (Invitrogen) at 1:1000 dilution.

4.5. Heat-shock induction

If not stated otherwise for heat-shock embryos were incubated for 1 h at 38 °C. 2 h after heat-treatment embryos were collected for total RNA preparation and fixation in 4% PFA for WISH.

4.6. Cycloheximide treatment

For translation inhibition cycloheximide (CHX, Calbiochem) was used as described (Negron and Lockshin, 2004). Embryos were exposed to 100 µg/ml of CHX starting 30 min after heat-shock induction and fixed for WISH 2 h after start of chemical treatment.

4.7. Functional kidney analysis

Functional kidney testing was performed according to Kramer-Zucker et al. (2005). Embryos were injected with Tetramethylrhodamin conjugated 70 kD dextran into the common cardinal vein at 3.5 dpf and embedded into 1.2% low melt agarose. Agarose surrounding the trunk was carefully removed with forceps. Excretion was monitored 5–30 min after dye injection at a Leica DM6000 microscope using a SPOT RT3 camera and Visitron software.

4.8. TEM sections

Animals were anaesthesized with MS222 and immediately fixed with glutaraldehyde and osmium tetroxide, postfixed with glutaraldehyde, osmium tetroxide and potassium dichromate according to Rombout (Rombout et al., 1978). Specimen were dehydrated in an acetone series and embedded in PolyBed 812. Ultrathin sections were cut with a Leica ultramicrotome UCT (Leica, Vienna), stained with lead citrate and examined with a Libra 120 energy filter transmission electron microscope (Zeiss, Germany) or a Philips CM 120 (F.E.I., the Netherlands). Images were acquired using an Olympus SiS iTEM 5.0 software and a TRS 2048 high speed camera (Troendle, Germany).

4.9. Transplantation experiments

Tg(hsp:mnx1-VP16;hsp:YFP) embryos were injected with Fluorescein-Dextran (Sigma) at the 1-cell-stage. Fluorescein-labeled cells were transplanted into wildtype animals at sphere stage. Embryos were heat-treated at the 5som stage and fixed in 4% PFA at the 8som stage. Staining of *irx1b* was performed by WISH. Visualization of Fluorescein-Dextran labeled cells was acquired using Anti-Fluorescein-POD antibodies (Roche) in a 1:1000 dilution and FITC substrate (Sigma).

4.10. Microarray analysis

Outcrosses of *Tg(hsp:mnx1;hsp:YFP)* and *Tg(hsp:mnx1-VP16;hsp:YFP)* were used to obtain identically treated samples of heterozygous transgenic (YFP^+) and control (YFP^-) embryos. Three biological samples were collected for each line. Heat-shock treatment was performed at the 12 somite stage (16hpf). After incubation for 45 min at 38 °C embryos were kept at 28 °C for additional 2 h (*Tg(hsp:mnx1-VP16;hsp:YFP)*) or 4 h (*Tg(hsp:mnx1;hsp:YFP)*). Longer incubation at 28 °C for *mnx1* induced embryos was due to the assumption that sufficient target gene repression would take longer than target gene activation. Embryos were then sorted for transgenic and control embryos and 50 embryos for each sample were collected for total RNA preparation using the RNAeasy kit from Quiagen. Remaining embryos were fixed for whole mount *in situ* hybridization analysis and ubiquitously increased *mnx1* expression confirmed successful transgenic induction. RNA samples of corresponding *in situ* hybridization (ISH) tested transgenic and control embryos were used for Microarray analysis.

The microarray was conducted at the Core Facility Genomics at the University of Freiburg using an Agilent 2100 Bioanalyzer. A two-color array was used for analysis. Calculations of the Core Facility group (Freiburg Center for Data Analysis and Modeling, Dr. Kurz) determined significantly regulated genes through additional combinatorial calculations of the *p*-value and corrected *p*-value and the absolute fold change. Multiple testing correction: Benjamini-Hochberg. Raw data were analyzed using the LIMMA-Package (Smyth et al., 2005; Wettenhall and Smyth, 2004). The red/green "Median Signal" from the AFE software was used as signal, the red/green "BGMedian Signal" as background. Background correction mode was "normexp" with an offset of 50, for normalization within arrays the "loess" option was used. Normalization between arrays was carried out with the "Aquantile" method.

4.11. Quantitative PCR

For qPCR analyses embryos were heat-treated at 15hpf and collected at 18hpf for total RNA preparation from YFP− control and YFP+ transgenic embryos (RNeasy kit, Qiagen). The cDNA samples were prepared with the First strand cDNA kit from Invitrogen. Real time PCR was performed on the ABI 7500 cycler (Applied Biosystems) using ABI Sybr Green reagent. As a standard control *ef1α* expression levels were analysed.

4.12. Microscopy analysis

For confocal microscopy analysis, the LSM510 (Zeiss) was used. Embryos were embedded in 1.2% low melting agarose (Biozym) dissolved in egg-water. Images were taken with the 20 × and 40 × water immersion objectives. Stacks were analyzed with the LSM Examiner (Zeiss) software. For brightfield images of whole mount *in situ* stainings the Leica MZ16FA microscope was used. Embryos were transferred to 100% glycerol for imaging. Figures were prepared using the Adobe Photoshop software.

4.13. Statistical analysis

Statistical analyses additional to Microarray analysis were

performed using the two-tailed, two sample Student's test and pValues <0.05 were considered significant. The GraphPad Prism 5 software was used for analysis.

GO term analyses of Microarray based differentially expressed genes was performed with the DAVID bioinformatics resources 6.7 (Huang da et al., 2009a, 2009b).

Acknowledgments

We are grateful to Robin Kimmel for suggestions and critical reading of the manuscript. We thank Sylvie Schneider-Maunoury for providing plasmids for *irx in situ* probes and Alan Davidson for pronephric tubule markers. Also, we thank Michael W. Hess for the use of the Philips CM 120 TEM. This project was supported by a Grant of the Austrian Science Foundation FWF (grant P 20492) to DM, the University Innsbruck and a Grant of the Tyrolean Science Foundation TWF (grant 0404/568) to E.O.

Appendix A. Supplementary information

Supplementary data associated with this article can be found in the online version at http://dx.doi.org/10.1016/j.ydbio.2015.10.014.

References

Alarcon, P., Rodriguez-Seguel, E., Fernandez-Gonzalez, A., Rubio, R., Gomez-Skarmeta, J.L., 2008. A dual requirement for Iroquois genes during Xenopus kidney development. Development 135, 3197–3207.
Bellefroid, E.J., Kobbe, A., Gruss, P., Pieler, T., Gurdon, J.B., Papalopulu, N., 1998. Xiro3 encodes a Xenopus homolog of the Drosophila Iroquois genes and functions in neural specification. EMBO J. 17, 191–203.
Belloni, E., Martucciello, G., Verderio, D., Ponti, E., Seri, M., Jasonni, V., Torre, M., Ferrari, M., Tsui, L.C., Scherer, S.W., 2000. Involvement of the HLXB9 homeobox gene in Currarino syndrome. Am. J. Hum. Genet. 66, 312–319.
Bosse, A., Zulch, A., Becker, M.B., Torres, M., Gomez-Skarmeta, J.L., Modolell, J., Gruss, P., 1997. Identification of the vertebrate Iroquois homeobox gene family with overlapping expression during early development of the nervous system. Mech. Dev. 69, 169–181.
Briscoe, J., Pierani, A., Jessell, T.M., Ericson, J., 2000. A homeodomain protein code specifies progenitor cell identity and neuronal fate in the ventral neural tube. Cell 101, 435–445.
Broihier, H.T., Skeath, J.B., 2002. Drosophila homeodomain protein dHb9 directs neuronal fate via crossrepressive and cell-nonautonomous mechanisms. Neuron 35, 39–50.
Brunskill, E.W., Aronow, B.J., Georgas, K., Rumballe, B., Valerius, M.T., Aronow, J., Kaimal, V., Jegga, A.G., Yu, J., Grimmond, S., McMahon, A.P., Patterson, L.T., Little, M.H., Potter, S.S., 2008. Atlas of gene expression in the developing kidney at microanatomic resolution. Dev. Cell 15, 781–791.
Catala, M., 2002. Genetic control of caudal development. Clin. Genet. 61, 89–96.
Cavodeassi, F., Modolell, J., Gomez-Skarmeta, J.L., 2001. The Iroquois family of genes: from body building to neural patterning. Development 128, 2847–2855.
Cheng, C.W., Yan, C.H., Choy, S.W., Hui, M.N., Hui, C.C., Cheng, S.H., 2007. Zebrafish homologue irx1a is required for the differentiation of serotonergic neurons. Dev. Dyn.: Off. Publ. Am. Assoc. Anat. 236, 2661–2667.
Colapinto, M.N., Vowinckel, E.A., Colapinto, N.D., 2003. Complete Currarino syndrome in an adult, presenting as a fecalith obstruction: report of a case. J. Can. Chir. 46, 303–306.
Cretolle, C., Zerah, M., Jaubert, F., Sarnacki, S., Revillon, Y., Lyonnet, S., Nihoul-Fekete, C., 2006. New clinical and therapeutic perspectives in Currarino syndrome (study of 29 cases). J. Pediatr. Surg. 41, 126–131, discussion 126–131.
Cretolle, C., Pelet, A., Sanlaville, D., Zerah, M., Amiel, J., Jaubert, F., Revillon, Y., Baala, L., Munnich, A., Nihoul-Fekete, C., Lyonnet, S., 2008. Spectrum of HLXB9 gene mutations in Currarino syndrome and genotype-phenotype correlation. Hum. Mutat. 29, 903–910.
Currarino, G., Coln, D., Votteler, T., 1981. Triad of anorectal, sacral, and presacral anomalies. AJR: Am. J. Roentgenol. 137, 395–398.
Dalgin, G., Ward, A.B., le, Hao, Beattie, T., Nechiporuk, C.E., Prince, V.E., A., 2011. Zebrafish mnx1 controls cell fate choice in the developing endocrine pancreas. Development 138, 4597–4608.
Deguchi, Y., Kehrl, J.H., 1991. Selective expression of two homeobox genes in CD34-positive cells from human bone marrow. Blood 78, 323–328.
Deguchi, Y., Yamanaka, Y., Theodossiou, C., Najfeld, V., Kehrl, J.H., 1993. High expression of two diverged homeobox genes, HB24 and HB9, in acute leukemias: molecular markers of hematopoietic cell immaturity. Leukemia 7, 446–451.
Drummond, I., 2003. Making a zebrafish kidney: a tale of two tubes. Trends Cell Biol. 13, 357–365.
Drummond, I.A., 2000. The zebrafish pronephros: a genetic system for studies of kidney development. Pediatr. Nephrol. 14, 428–435.
Eisen, J.S., 1999. A case of mistaken identity. Neuron 23, 626–627.
Gerlach, G.F., Wingert, R.A., 2013. Kidney organogenesis in the zebrafish: insights into vertebrate nephrogenesis and regeneration. Wiley interdisciplinary reviews. Dev. Biol. 2, 559–585.
Gerlach, G.F., Wingert, R.A., 2014. Zebrafish pronephros tubulogenesis and epithelial identity maintenance are reliant on the polarity proteins Prkc iota and zeta. Dev. Biol. 396, 183–200.
Gomez-Skarmeta, J.L., Modolell, J., 2002. Iroquois genes: genomic organization and function in vertebrate neural development. Curr. Opin. Genet. Dev. 12, 403–408.
Haas, P., Gilmour, D., 2006. Chemokine signaling mediates self-organizing tissue migration in the zebrafish lateral line. Dev. Cell 10, 673–680.
Harrison, K.A., Druey, K.M., Deguchi, Y., Tuscano, J.M., Kehrl, J.H., 1994. A novel human homeobox gene distantly related to proboscipedia is expressed in lymphoid and pancreatic tissues. J. Biol. Chem. 269, 19968–19975.
Harrison, K.A., Thaler, J., Pfaff, S.L., Gu, H., Kehrl, J.H., 1999. Pancreas dorsal lobe agenesis and abnormal islets of Langerhans in Hlxb9-deficient mice. Nat. Genet. 23, 71–75.
Hauptmann, G., Gerster, T., 2000. Multicolor whole-mount in situ hybridization. Methods Mol. Biol. 137, 139–148.
Heliot, C., Desgrange, A., Buisson, I., Prunskaite-Hyyrylainen, R., Shan, J., Vainio, S., Umbhauer, M., Cereghini, S., 2013. HNF1B controls proximal-intermediate nephron segment identity in vertebrates by regulating Notch signalling components and Irx1/2. Development 140, 873–885.
Hollington, P., Neufing, P., Kalionis, B., Waring, P., Bentel, J., Wattchow, D., Tilley, W. D., 2004. Expression and localization of homeodomain proteins DLX4, HB9 and HB24 in malignant and benign human colorectal tissues. Anticancer Res. 24, 955–962.
Houweling, A.C., Dildrop, R., Peters, T., Mummenhoff, J., Moorman, A.F., Ruther, U., Christoffels, V.M., 2001. Gene and cluster-specific expression of the Iroquois family members during mouse development. Mechan. Dev. 107, 169–174.
Huang da, W., Sherman, B.T., Lempicki, R.A., 2009a. Bioinformatics enrichment tools: paths toward the comprehensive functional analysis of large gene lists. Nucleic Acids Res. 37, 1–13.
Huang da, W., Sherman, B.T., Lempicki, R.A., 2009b. Systematic and integrative analysis of large gene lists using DAVID bioinformatics resources. Nat. Protoc. 4, 44–57.
Iyer, R.S., Khanna, P.C., 2010. Currarino syndrome. Pediatr. Radiol. 40 (Suppl 1), S102.
Jessell, T.M., 2000. Neuronal specification in the spinal cord: inductive signals and transcriptional codes. Nat. Rev. Genet. 1, 20–29.
Kimmel, C.B., Ballard, W.W., Kimmel, S.R., Ullmann, B., Schilling, T.F., 1995. Stages of embryonic development of the zebrafish. Dev. Dyn.: Off. Publ. Am. Assoc. Anat. 203, 253–310.
Kimmel, R.A., Onder, L., Wilfinger, A., Ellertsdottir, E., Meyer, D., 2011. Requirement for Pdx1 in specification of latent endocrine progenitors in zebrafish. BMC Biol. 9, 75.
Kochling, J., Karbasiyan, M., Reis, A., 2001. Spectrum of mutations and genotype-phenotype analysis in Currarino syndrome. Eur. J. Hum. Genet.: EJHG 9, 599–605.
Kramer-Zucker, A.G., Olale, F., Haycraft, C.J., Yoder, B.K., Schier, A.F., Drummond, I.A., 2005. Cilia-driven fluid flow in the zebrafish pronephros, brain and Kupffer's vesicle is required for normal organogenesis. Development 132, 1907–1921.
Lange, K., 2011. Fundamental role of microvilli in the main functions of differentiated cells: outline of an universal regulating and signaling system at the cell periphery. J. Cell. Physiol. 226, 896–927.
Lecaudey, V., Anselme, I., Dildrop, R., Ruther, U., Schneider-Maunoury, S., 2005. Expression of the zebrafish Iroquois genes during early nervous system formation and patterning. J. Comp. Neurol. 492, 289–302.
Lee, S., Lee, B., Joshi, K., Pfaff, S.L., Lee, J.W., Lee, S.K., 2008. A regulatory network to segregate the identity of neuronal subtypes. Dev. Cell 14, 877–889.
Lee, S.K., Jurata, L.W., Funahashi, J., Ruiz, E.C., Pfaff, S.L., 2004. Analysis of embryonic motoneuron gene regulation: derepression of general activators function in concert with enhancer factors. Development 131, 3295–3306.
Li, H., Arber, S., Jessell, T.M., Edlund, H., 1999. Selective agenesis of the dorsal pancreas in mice lacking homeobox gene Hlxb9. Nat. Genet. 23, 67–70.
Lynch, S.A., Wang, Y., Strachan, T., Burn, J., Lindsay, S., 2000. Autosomal dominant sacral agenesis: currarino syndrome. J. Med. Genet. 37, 561–566.
Marra, A.N., Wingert, R.A., 2014. Roles of Iroquois transcription factors in kidney development. Cell Dev. Biol. 3, 1000131.
Massa, F., Garbay, S., Bouvier, R., Sugitani, Y., Noda, T., Gubler, M.C., Heidet, L., Pontoglio, M., Fischer, E., 2013. Hepatocyte nuclear factor 1beta controls nephron tubular development. Development 140, 886–896.
Mitra, S., Lukianov, S., Ruiz, W.G., Cianciolo Cosentino, C., Sanker, S., Traub, L.M., Hukriede, N.A., Apodaca, G., 2012. Requirement for a uroplakin 3a-like protein in the development of zebrafish pronephric tubule epithelial cell function, morphogenesis, and polarity. PloS One 7, e41816.
Muhr, J., Andersson, E., Persson, M., Jessell, T.M., Ericson, J., 2001. Groucho-mediated transcriptional repression establishes progenitor cell pattern and neuronal fate in the ventral neural tube. Cell 104, 861–873.
Negron, J.F., Lockshin, R.A., 2004. Activation of apoptosis and caspase-3 in zebrafish early gastrulae. Dev. Dyn.: Off. Publ. Am. Assoc. Anat. 231, 161–170.
Obara, T., Mangos, S., Liu, Y., Zhao, J., Wiessner, S., Kramer-Zucker, A.G., Olale, F.,

Schier, J., Drummond, I.A., 2006. Polycystin-2 immunolocalization and function in zebrafish. J. Am. Soc. Nephrol.: JASN 17, 2706–2718.
Pickles, S., Cadieux-Dion, M., Alvarez, J.I., Lecuyer, M.A., Peyrard, S.L., Destroismaisons, L., St-Onge, L., Terouz, S., Cossette, P., Prat, A., Vande Velde, C., 2013. Endo-MitoEGFP mice: a novel transgenic mouse with fluorescently marked mitochondria in microvascular endothelial cells. PloS One 8, e74603.
Raschperger, E., Neve, E.P., Wernerson, A., Hultenby, K., Pettersson, R.F., Majumdar, A., 2008. The coxsackie and adenovirus receptor (CAR) is required for renal epithelial differentiation within the zebrafish pronephros. Dev. Biol. 313, 455–464.
Reggiani, L., Raciti, D., Airik, R., Kispert, A., Brandli, A.W., 2007. The prepattern transcription factor Irx3 directs nephron segment identity. Genes Dev. 21, 2358–2370.
Rodriguez-Seguel, E., Alarcon, P., Gomez-Skarmeta, J.L., 2009. The Xenopus Irx genes are essential for neural patterning and define the border between prethalamus and thalamus through mutual antagonism with the anterior repressors Fezf and Arx. Dev. Biol. 329, 258–268.
Rombout, J.H., Lamers, C.H., Hanstede, J.G., 1978. Enteroendocrine APUD cells in the digestive tract of larval Barbus conchonius (Teleostei, Cyprinidae). J. Embryol. Exp. Morphol. 47, 121–135.
Ross, A.J., Ruiz-Perez, V., Wang, Y., Hagan, D.M., Scherer, S., Lynch, S.A., Lindsay, S., Custard, E., Belloni, E., Wilson, D.I., Wadey, R., Goodman, F., Orstavik, K.H., Monclair, T., Robson, S., Reardon, W., Burn, J., Scambler, P., Strachan, T., 1998. A homeobox gene, HLXB9, is the major locus for dominantly inherited sacral agenesis. Nat. Genet. 20, 358–361.
Saha, M.S., Miles, R.R., Grainger, R.M., 1997. Dorsal-ventral patterning during neural induction in Xenopus: assessment of spinal cord regionalization with xHB9, a marker for the motor neuron region. Dev. Biol. 187, 209–223.
Seredick, S.D., Van Ryswyk, L., Hutchinson, S.A., Eisen, J.S., 2012. Zebrafish Mnx proteins specify one motoneuron subtype and suppress acquisition of interneuron characteristics. Neural Dev. 7, 35.
Serluca, F.C., Fishman, M.C., 2001. Pre-pattern in the pronephric kidney field of zebrafish. Development 128, 2233–2241.
Smyth, G.K., Michaud, J., Scott, H.S., 2005. Use of within-array replicate spots for assessing differential expression in microarray experiments. Bioinformatics 21, 2067–2075.
Stedman, A., Lecaudey, V., Havis, E., Anselme, I., Wassef, M., Gilardi-Hebenstreit, P., Schneider-Maunoury, S., 2009. A functional interaction between Irx and Meis patterns the anterior hindbrain and activates krox20 expression in rhombomere 3. Dev. Biol. 327, 566–577.
Sullivan-Brown, J., Schottenfeld, J., Okabe, N., Hostetter, C.L., Serluca, F.C., Thiberge, S.Y., Burdine, R.D., 2008. Zebrafish mutations affecting cilia motility share similar cystic phenotypes and suggest a mechanism of cyst formation that differs from pkd2 morphants. Dev. Biol. 314, 261–275.
Thaler, J., Harrison, K., Sharma, K., Lettieri, K., Kehrl, J., Pfaff, S.L., 1999. Active suppression of interneuron programs within developing motor neurons revealed by analysis of homeodomain factor HB9. Neuron 23, 675–687.
Thisse, C., Thisse, B., Schilling, T.F., Postlethwait, J.H., 1993. Structure of the zebrafish snail1 gene and its expression in wild-type, spadetail and no tail mutant embryos. Development 119, 1203–1215.
Vasilyev, A., Liu, Y., Hellman, N., Pathak, N., Drummond, I.A., 2012. Mechanical stretch and PI3K signaling link cell migration and proliferation to coordinate epithelial tubule morphogenesis in the zebrafish pronephros. PloS One 7, e39992.
Vasilyev, A., Liu, Y., Mudumana, S., Mangos, S., Lam, P.Y., Majumdar, A., Zhao, J., Poon, K.L., Koondrychyn, I., Korzh, V., Drummond, I.A., 2009. Collective cell migration drives the morphogenesis of the kidney nephron. PloS Biol. 1, e1000009.
Warga, R.M., Kane, D.A., Ho, R.K., 2009. Fate mapping embryonic blood in zebrafish: multi- and unipotential lineages are segregated at gastrulation. Dev. Cell 16, 744–755.
Wendik, B., Maier, E., Meyer, D., 2004. Zebrafish mnx genes in endocrine and exocrine pancreas formation. Dev. Biol. 268, 372–383.
Wettenhall, J.M., Smyth, G.K., 2004. limmaGUI: a graphical user interface for linear modeling of microarray data. Bioinformatics 20, 3705–3706.
Wildenhain, S., Ingenhag, D., Ruckert, C., Degistirici, O., Dugas, M., Meisel, R., Hauer, J., Borkhardt, A., 2012. Homeobox protein HB9 binds to the prostaglandin E receptor 2 promoter and inhibits intracellular cAMP mobilization in leukemic cells. J. Biol. Chem. 287, 40703–40712.
Wilkens, L., Jaggi, R., Hammer, C., Inderbitzin, D., Giger, O., von Neuhoff, N., 2011. The homeobox gene HLXB9 is upregulated in a morphological subset of poorly differentiated hepatocellular carcinoma. Virchows Arch.: Int. J. Pathol. 458, 697–708.
William, C.M., Tanabe, Y., Jessell, T.M., 2003. Regulation of motor neuron subtype identity by repressor activity of Mnx class homeodomain proteins. Development 130, 1523–1536.
Wingert, R.A., Davidson, A.J., 2008. The zebrafish pronephros: a model to study nephron segmentation. Kidney Int. 73, 1120–1127.
Wingert, R.A., Davidson, A.J., 2011. Zebrafish nephrogenesis involves dynamic spatiotemporal expression changes in renal progenitors and essential signals from retinoic acid and irx3b. Dev. Dyn.: Off. Publ. Am. Assoc. Anat. 240, 2011–2027.
Wingert, R.A., Selleck, R., Yu, J., Song, H.D., Chen, Z., Song, A., Zhou, Y., Thisse, B., Thisse, C., McMahon, A.P., Davidson, A.J., 2007. The cdx genes and retinoic acid control the positioning and segmentation of the zebrafish pronephros. PLoS Genet. 3, 1922–1938.
Zhang, Q., Liu, Q., Austin, C., Drummond, I., Pierce, E.A., 2012. Knockdown of ttc26 disrupts ciliogenesis of the photoreceptor cells and the pronephros in zebrafish. Mol. Biol. Cell 23, 3069–3078.
Zhao, C., Malicki, J., 2007. Genetic defects of pronephric cilia in zebrafish. Mech. Dev. 124, 605–616.